https://doi.org/10.1680/jenge.17.00093

# A HETEROGENEOUS BENTONITE BARRIER AFTER 18 YEARS OPERATION: FINAL PHYSICAL STATE OF THE BENTONITE BARRIER OF THE FEBEX IN SITU TEST

Author 1

- María Victoria Villar, Ph.D.
- Centro de Investigaciones Energéticas, Medioambientales y Tecnológicas (CIEMAT), Madrid, Spain
- 0000-0002-7282-5613

Author 2

- Rubén J. Iglesias
- Centro de Investigaciones Energéticas, Medioambientales y Tecnológicas (CIEMAT), Madrid, Spain

Author 3

- José Luis García-Siñeriz
- Amberg Infraestructuras S.A., Madrid, Spain,

**Corresponding author contact details**:

Avd. Complutense 40, 28040 Madrid, Spain, mv.villar@ciemat.es, ph: +34913466391, fax: +34913466542

## Abstract

The FEBEX *in situ* experiment was a full-scale test reproducing the near-field of a nuclear waste repository. It was performed in a gallery excavated in granite, with a heater whose surface temperature was set to100°C simulating the waste canister and a bentonite barrier composed of highly-compacted blocks. The test was completely dismantled after eighteen years of operation. Numerous samples of bentonite were taken for the on-site determination of dry density and water content.

The on-site measurements showed that the physical state of the barrier was very much affected by the processes to which it had been subjected, namely hydration with the granite groundwater and/or thermal gradient. Although the degree of saturation of the bentonite was overall quite high, there were important water content and dry density gradients everywhere in the barrier, but steeper around the heater. These gradients did not impair the performance of the barrier, but imply that the barrier can be irreversibly inhomogeneous.

**Keywords**: radioactive waste disposal, Fabric/structure of soils, Cut-off walls & barriers

## 1. Introduction

The system of barriers (sealing and backfill materials) in a deep geological repository for high-level radioactive waste aims to prevent the possible escape paths for radionuclides to the environment, the most important of which is the circulation of groundwaters. The sealing materials (buffers) will be in contact with the waste containers and their basic functions are to prevent or limit the entry of water to the wastes and to contribute to radionuclide retention. Other additional functions are to contribute to heat dissipation and to provide mechanical protection for the waste canisters (*e.g.* Chapman & McCombie 2003, Vardon & Heimovaara 2017).

In this context, the aim of the FEBEX project (Full-scale Engineered Barriers Experiment) was to study the behaviour of components in the near-field of a repository in crystalline rock according to the Spanish reference concept for geological disposal of nuclear waste. As part of this project an *in situ* test, under natural conditions and at full scale, was performed at the Grimsel Test Site (Switzerland), an underground laboratory managed by NAGRA (the Swiss agency for nuclear waste management). In addition to a purely demonstration aim, this *in situ* test allowed to monitor thermo-hydro-mechanical (THM) changes in a bentonite barrier in response to groundwater interaction and to heat release from a simulated nuclear waste disposal canister. A 70-m long gallery of 2.3 m in diameter was excavated through the granite and two heaters simulating the thermal effect of the wastes –with dimensions and weights analogous to

those of the real canisters– were placed inside a perforated steel liner installed concentrically with the gallery and surrounded by a barrier of highly-compacted bentonite blocks (Figure 1). The gallery was closed by a concrete plug. The FEBEX *in situ* test was initially monitored with 632 sensors of very diverse types, installed to track the different thermo-hydro-mechanical processes that occurred in both the clay barrier and the surrounding rock throughout the entire life of the test. The THM monitoring and heater control system were managed remotely from Madrid. The maximum external surface temperature of the heaters was set to 100°C and the bentonite barrier was naturally hydrated by the granitic groundwater (ENRESA, 2006).

The clay barrier was built with compacted bentonite blocks arranged in vertical slices with three concentric rings around the heaters (Figure 2). The thickness of the bentonite barrier in the heater areas was 65 cm (distance from liner to granite). The blocks were obtained by uniaxial compaction of the FEBEX clay with its hygroscopic water content (14%) at pressures of between 40 and 45 MPa, what gave place to dry densities of 1.69-1.70 g/cm$^3$. The initial dry density of the blocks was selected by taking into account the volume of the construction gaps and the need to have a barrier with an average dry density of 1.60 g/cm$^3$.

The heating stage of the *in situ* test began in February 1997. After five years of uninterrupted heating at constant temperature, the heater closer to the gallery entrance (Heater #1) was switched off. The concrete plug closing the gallery was then demolished. At the moment of dismantling in 2002, the pressure exerted by the bentonite towards this plug was of about 1 MPa at the axis of the gallery, and between 3.6 and 4.6 MPa in the middle part of the barrier (AITEMIN 2003). In the following months Heater #1 and all the bentonite and instruments preceding and surrounding it were extracted, except for one metre of bentonite slices in front of the back lid of Heater #1 (Bárcena et al. 2003). During dismantling a net forward movement of the bentonite barrier towards the entrance of the gallery (of between 2 and 5 cm) was observed and measured. The 1-m long void left by the final part of Heater #1 was filled with a dummy steel empty canister and the remaining part of the experiment was sealed with a new sprayed shotcrete plug (Figure 3). It is considered that this milestone, after all the activities related to the

partial dismantling had ended, was the beginning of the second operational phase. However, Heater #2 was in operation at all times during the partial dismantling. The disturbance caused by the partial dismantling on the remaining part of the experiment was very small (Bárcena et al. 2003). Although some displacement of the buffer towards the gallery entrance was observed, the readings of the sensors left in place showed a fast recovery of the pressures after construction of the new plug. No significant alterations were observed in other parameters, such as temperature or humidity.

After eighteen years of operation (Lanyon & Gaus 2016), the FEBEX Dismantling Project (FEBEX-DP) undertook the dismantling of the experiment (García-Siñeriz et al. 2016). Heater #2 was switched off in April 2015, the shotcrete plug was demolished and 14 days after heater shutdown the buffer removal and sampling started. In particular, samples were taken to determine on site their water content and dry density, with the aim of assessing the final state of the barrier (Villar et al. 2016). This paper summarises and discusses the results obtained during dismantling concerning the physical state of the bentonite barrier. Its relevance arises from the fact that, up to the whole dismantling of the FEBEX *in situ* test, no bentonite subjected to repository conditions for such a long period of time had ever been studied.

## 2. Engineered Barrier Material

The material used to construct the engineered barrier was the FEBEX bentonite, extracted from the Cortijo de Archidona quarry in SE Spain. At the factory, the clay was disaggregated and gently dried to a water content of around 14%, all the material of particle size greater than 5 mm being rejected. The processed material was used for fabrication of the blocks for the large-scale test and for the laboratory tests performed for the characterization of the clay. The physico-chemical properties of the FEBEX bentonite, as well as its most relevant thermo-hydro-mechanical and geochemical characteristics were summarised in ENRESA (2006).

The montmorillonite content of the FEBEX bentonite is above 90 wt.% (92±3 %). Besides, the bentonite contains variable quantities of quartz (2±1 wt.%), plagioclase (3±1 wt.%), K-felspar

(traces), calcite (1±0.5 wt.%), and cristobalite-trydimite (2±1 wt.%). The cation exchange capacity of the smectite is 102±4 meq/100g, the main exchangeable cations being calcium (35±2 meq/100g), magnesium (31±3 meq/100g) and sodium (27±1 meq/100g). The predominant soluble ions are chloride, sulphate, bicarbonate and sodium.

The liquid limit of the bentonite is 102±4%, the plastic limit 53±3%, the density of the solid particles 2.70±0.04 g/cm$^3$, and 67±3% of particles are smaller than 2 µm. The hygroscopic water content in equilibrium with the laboratory atmosphere is 13.7±1.3%.

The swelling pressure ($P_s$, MPa) of FEBEX samples flooded with deionised water up to saturation at room temperature and constant volume conditions can be related to dry density ($\rho_d$, g/cm$^3$) through the following equation (Villar 2002):

$$\ln P_s = 6.77\rho_d - 9.07 \quad [1]$$

## 3. State of the barrier during operation

In spite of the long duration of the experiment and the short life expectancy of the sensors guaranteed by the manufacturers, at the moment the barrier was dismantled many sensors were still providing information and continued doing so during the dismantling operations (Martínez et al. 2016). Figure 4 shows the steady temperatures measured by thermocouples at different instrumented sections in the bentonite barrier (see Figure 3 for location of sections along the gallery). The temperatures are plotted as a function of the distance to the gallery axis, i.e. in radial direction. Obviously, there is a clear difference between the temperatures measured in sections around the heater and those away from it. The sections around the heater showed a steep temperature gradient, with temperatures between 100°C in the contact with the liner and higher than 34°C close to the granite, whereas the bentonite sections located away from the influence of the heater had lower and more homogeneous temperatures. Thus, in section S38, at 100 cm from the front lid of the heater, the temperatures were 35±5°C, and in section S62, at

275 cm from the back lid of the heater, the temperature was of 22°C. Around the heater the temperatures were higher in the middle part of it (sections S45 to S51), because the heat loss was larger at the heater ends. This feature is highlighted in Figure 5, where the temperatures have been plotted as a function of the *x*-coordinate, whose origin is indicated in Figure 1. Hence, during operation the temperatures in the barrier decreased from the middle part of the heater towards the front and the back of the gallery. Also, although it cannot be appreciated in these Figures, the temperatures in vertical sections around the heater were slightly higher at the lower part of the bentonite barrier, thanks to the better thermal contact between heater, liner and bentonite.

The operational relative humidity measurements, which are related to the degree of water saturation of the clay, gave values of 100% at the time of dismantling in the intermediate and external rings of the barrier. The relative humidity sensors located close to the heater had failed long before dismantling. The total pressure recordings, which are also related to the degree of saturation of the bentonite, since swelling pressure tends to increase with rising degree of saturation, showed at the time of dismantling mostly an increasing trend. The axial pressure at the shotcrete/bentonite contact as measured by two cells placed in the middle ring of the barrier was about 6 MPa, similar to the axial pressure measured by a cell placed at the gallery axis between the back of the dummy canister and the bentonite (section S38 in Figure 3). An axial pressure close to 6 MPa was recorded at the back of the gallery, between the rock and the bentonite (section S62). Also, in the middle part of the heater (section S48), the radial pressure at the rock/bentonite contact was higher than 6 MPa. These values would correspond to the swelling pressure of saturated bentonite of dry density 1.58-1.61 g/cm$^3$ (Eq. 1). However, the cells located in the intermediate ring of sections S42 (front of heater) and S48 (middle of heater) were recording at the moment of dismantling tangential and radial values between 1 and 2 MPa, which are far from the equilibrium pressure expected for the average dry density of the barrier and would confirm that full saturation had not been reached.

## 4. Dismantling of the bentonite barrier

The bentonite dismantling operations took three months and started after the heater had been switched off for 14 days. Upon heater shutdown the temperatures dropped, and were below 30°C at all points in the barrier when it started to be dismantled. Consequently, when the bentonite sections were dismantled the temperature in them was lower than during operation. In particular, the heater had been switched off between 24 and 97 days before dismantling sections S37 and S61, respectively. The change in temperature during this time was of a few degrees (4-8°C) for the sections farther away from the heater, and up to 80°C in the bentonite closest to the liner in the middle part of the heater. Figure 6 shows the evolution of temperature as measured by the thermocouples placed in instrumented section S54, located at the back end of the heater (Figure 3). During this time changes took probably place in the bentonite, and hence the state observed upon dismantling did not exactly reflect the state of the barrier during operation. This aspect is discussed in 5.3.

Upon removal of the shotcrete plug and exposure of the bentonite slices, it was observed that all the construction gaps between blocks had sealed, both those among blocks of the same section and the gaps between bentonite slices (Figure 2, right). This was evidenced by the difficulty found in separating sampling sections. The granite/bentonite contact was also tight at all locations and the gaps hewn in the blocks to allow for the passing of cables had been completely filled by the swelling of the bentonite. These observations were already done during the partial dismantling after five years operation (Villar et al. 2005, 2006). Another remarkable feature noticed during dismantling was the intrusion of bentonite through the liner holes, particularly in the upper part of the heater, where there was a gap between liner and heater (Figure 7, left). All these observations done during dismantling are documented in detail in Kober & van Meir (2017).

During dismantling, and prior to sampling, the position of the slices with respect to the origin of coordinates (indicated in Figure 1) was measured using a laser distance-meter with an accuracy of ±5 mm (García-Siñeriz et al. 2016). These measurements were done at five different points

on the surface of the section. The final position of the slices was also checked with a metric tape fixed to the middle left side of the gallery during installation of the experiment in 1997. These measurements agreed well with the laser's ones (Villar et al. 2016) and both allowed to check changes between the installation coordinate of every section (as built) and the final coordinate. Differences between the two would imply movement of the barrier along the gallery. In fact, two kinds of movement were detected, one of them probably took place during operation and the other one during dismantling:

- Most slices moved towards the entrance of the gallery, particularly those closest to the shotcrete plug. In the front part of the barrier the displacement was as high as 50 mm and decreased with distance into the gallery. This displacement towards the gallery entrance took probably place as the shotcrete plug was demolished and the pressure released. The axial stresses measured on the shotcrete plug just before the start of the dismantling operations were 6 MPa (Martínez et al. 2016). Up to approximately the *x*-coordinate 14.8 m, the average displacement was of 20 mm.

- From that point to the back of the gallery, the slices had moved in the opposite direction, towards the back of the gallery, more significantly as the slice was closest to the rearmost part of the gallery. This backward movement, which took place during operation, is analysed below in 5.2.2.

The observations on site confirmed this displacement: the external part of the blocks of the outer ring showed frequently grooves in the direction of the gallery axis, caused by the friction with the uneven surface of the granite, whereas the granite surface was covered by a film of bentonite showing striation parallel to the gallery axis (Figure 7, right). This had an appearance similar to slickensides observed in geological formations (Kober & van Meir 2017).

During dismantling many samples of the different components of the installation (bentonite, sensors, liner, granite, etc.) were taken and sent to different laboratories for analysis (Bárcena & García-Siñeriz 2015). Also, for the determination of water content and dry density of the bentonite on site, in each of the sampling sections shown in Figure 3, samples were taken

following six radii separated by 60° and named clockwise from A (the upper radius) to F, as indicated in Figure 2. The bentonite blocks preceding the sampling radii were removed just before sampling, in order to prevent changes in the bentonite water content. Each section was usually sampled within a day. The samples were obtained by drilling the bentonite following a template with a crown drill bit. In the sections around the liner, six samples were taken along each radius, and in those without liner, ten or eleven samples were taken along each radius. The cylindrical samples had a length of 6 cm and a diameter of 4.8 cm. They were immediately wrapped in plastic foil and taken to an on-site laboratory.

The conditions in the service area of the FEBEX gallery during the bentonite dismantling period were 86.4±7.7% for the relative humidity and 15.8±0.5°C for the temperature.

# 5. On site measurements

## 5.1 Methodology

Once in the on-site lab each sample was cut and trimmed into two subsamples each of between 5 and 37 $cm^3$ volume (average volume 18 $cm^3$) and masses of between 10 and 75 g (average mass 35 g). The external part of the subsamples that had been in contact with the crown drill bit was removed and the surfaces smoothed. In each of these subsamples water content and dry density were determined.

The gravimetric water content ($w$) is defined as the ratio between the mass of water and the mass of dry solid expressed as a percentage. The mass of water was determined as the difference between the mass of the sample and its mass after oven drying at 110°C for 48 h (mass of dry solid). The precision of this measurement is about 0.2%. Dry density ($\rho_d$) is defined as the ratio between the mass of the dry sample and the volume occupied by it prior to drying. The volume of the specimens was determined by immersing them in a vessel containing mercury and by weighing the mercury displaced, considering for the calculation of volume a mercury density of 13.6 $g/cm^3$. The precision of this measurement is between 0.01 and 0.02

236 g/cm$^3$. The same samples whose volumes had been determined were used for the water content
237 determination (García-Siñeriz et al. 2016).

## 238 5.2 Results

239 Some representative results obtained on site are presented below, plotted for each sampling
240 section as a function of the distance to the gallery axis. In these plots, the values obtained in the
241 two subsamples per core are shown. The average values of these two subsamples were used to
242 obtain the 2-D plots for water content, dry density and degree of saturation of the sections.
243 These plots were obtained with the contour mapping software Surfer® using the Kriging
244 gridding method.

### 245 5.2.1 Vertical cross sections

246 The water content at all points in the barrier, even those close to the heater, was higher than the
247 initial one, i.e. greater than 14%. As an example, Figure 8 and Figure 9 show the water content
248 and dry density measured in sections S49 and S58, respectively. The first one was located
249 around the middle part of the heater, where, according to the sensors measurements, the
250 temperature during operation was approximately between 100 and 36°C (Figure 4). S58 was
251 located at 132 cm from the back of the heater, and consequently the temperatures in this section
252 during operation where lower and more homogeneous (Figure 5). The two figures show that
253 overall, the six radii sampled in each section yielded the same water content and dry density
254 distribution, which reveals the radial symmetry around the axis of the gallery for these state
255 properties. The same observation was done in all the other sections sampled, in most of them
256 the differences among the six sampled radii were negligible, particularly in terms of water
257 content. This feature would also confirm that the gaps between blocks were not preferential
258 pathways for water, which was already checked by detailed measurements during the partial
259 dismantling in 2002 (Villar et al. 2005, 2006). The higher water content and lower dry density
260 of the external part of some radii could be related to granite geological features (veins, fractures)
261 that could have supplied more water. On the other hand, the higher densities measured in radii

D and E (and slightly lower water contents) in section S49 (and S45, see below) were likely related to the higher temperature at the lower part of the barrier, where there was a better thermal contact, and consequently heat conduction, between heater, liner and bentonite.

The radial symmetry of these distribution patterns allows interpolating isolines in 2-D graphs, such as those shown in Figure 10 and Figure 11, where the water content and dry density, respectively, in a hot and a cold section can be seen. The reason for these strong gradients is the high swelling capacity of the bentonite: the external part of the barrier, in contact with the granite, took first water and swelled, pushing towards the rigid granite and generating a swelling pressure that, at the moment of dismantling was about 5 MPa at the rock/clay contact. At the same time the expanding bentonite pressed also inwards, where the clay was more deformable. The pressure inwards reduced the void ratio of the internal part of the barrier. As might be expected, the bentonite swelled also in the longitudinal direction, along the gallery axis, an aspect discussed in the following chapter. Around the heater the increase in dry density was enhanced by the water loss and associated shrinkage. The water from the hottest areas would migrate in the vapour phase towards cooler parts of the barrier and condense in the middle part of it. This is the reason why the water content and density gradients were more noticeable in those sections affected by the heater. The lower water content around the heater was identifiable upon dismantling as lighter colours of the internal ring of the barrier. The inwards radial movement of the barrier was also evinced during dismantling by the intrusion of bentonite through the liner holes (Figure 7, left).

From the contour plots of each sampling section the average values of each parameter have been computed by the mapping software and are shown in Table 1. Besides, taking into account the radial symmetry of the water content and dry density distributions, the average values of these variables in a vertical section have been obtained by fitting polynomial functions to represent their variation with the distance to the gallery axis, following the procedure used by Daucausse & Lloret (2002) and published in Villar et al. (2005). The values obtained are also shown in Table 1. The two methodologies gave similar values, with differences below the accuracy of the

289 methods used to determine water content and dry density. The degrees of saturation computed
290 taking for the bentonite a solid specific weight of 2.70 g/cm$^3$ and a density for the adsorbed
291 water of 1 g/cm$^3$ are also shown in the Table.

292 The values in the Table highlight the lower average water content and higher dry density of the
293 sections around the heater (S43 to S52), as well as the decrease of dry density towards the back
294 of the gallery. Figure 12 shows a direct comparison of the water content and dry density
295 measured in a section around the heater (S45) and away from it (S58). The data are the same as
296 those plotted in Figure 8 and Figure 9. It is remarkable that the water content in the external part
297 of the barrier, the 20 cm closest to the granite, was only slightly higher in the cold section than
298 in the section around the heater, whereas the main difference between the two was found in the
299 internal part of the barrier, where the water contents of the cold section were significantly
300 higher. The same kind of difference was observed concerning dry density. The larger
301 divergence between the dry densities of the two sections occurred in the internal part of the
302 barrier, although the densities in the hot section for a given distance to the gallery axis were in
303 all cases higher than those in the cold section. This can be related to the density changes along
304 the gallery observed in Table 1: the overall dry density of the barrier decreased towards the back
305 of the gallery, and section S58 was located much closer to the rear part of the gallery than
306 section S45. These longitudinal changes are discussed in the following section.

307 ### 5.3.2 Longitudinal sections

308 Thanks to the even distribution of sampling sections along the axis of the gallery (Figure 3) it
309 was possible to draw contour maps of longitudinal sections along the gallery axis for water
310 content and dry density. Figure 13 and Figure 14 show vertical longitudinal sections for water
311 content and dry density, respectively. These longitudinal profiles show clearly the lower water
312 content and higher dry density around the heater discussed in the previous section, but also that
313 the back of the gallery had the highest water contents and the lowest dry densities. The highest
314 dry densities were found around the rear half of the heater, whereas around the dummy canister
315 dry densities below the average of the barrier were observed. From these contour plots the

316 average values for each parameter can be computed. According to these values, the final
317 average water content, dry density and degree of saturation of the entire clay barrier would be
318 25.5%, 1.59 g/cm$^3$ and 97%, respectively.

319 The longitudinal inhomogeneities are highlighted when the values in Table 1 are plotted as a
320 function of the *x*-coordinate (Figure 15). As noted previously, the highest water content and
321 lowest dry density were found at the back of the gallery. The fact that the gallery had a concave
322 shape at its rear part made it difficult to fill it with bentonite blocks during installation of the
323 barrier. As a result the percentage of construction voids in the area was very high: 37% for the
324 three bentonite slices placed first *vs*. an average along the barrier of 5.5%. This would have
325 contributed to the conditions observed at the back of the test tunnel, since the higher porosity
326 would have allowed a larger volume of water to be taken. Also, the hydration surface at the
327 back of the gallery was larger, because the whole granite circular surface was supplying water,
328 which would have made the initial hydration quicker. At the same time, the bentonite slices
329 neighbouring those at the back of the gallery, i.e. those with an initial gap volume similar to that
330 in the rest of the experiment but away from the influence of the heater, upon initial water intake,
331 would have swollen preferentially towards the back of the gallery, where the void volume was
332 larger and the clay more deformable. These slices would be those located approximately
333 between *x*-coordinates 800 and 870 mm, i.e. between sampling sections S58 and S61, and in this
334 region a sharp decrease in dry density towards the back of the gallery took place, as can be
335 observed in Figure 14 and Figure 15. As commented above, the movement of these slices
336 towards the back of the gallery was confirmed by the difference between the initial *x*-coordinate
337 measured during installation and the one measured during dismantling.

338 On the other hand, the lowest water content and highest dry density were found around the
339 heater, particularly in its middle part, and at the bottom where the temperatures were slightly
340 higher during operation. Clearly, the thermal gradient hindered, or at least delayed, saturation.
341 The effect of thermal gradient affected the water content and dry density distribution in vertical
342 sections around the heater, as has already been discussed above, but also conditioned the

changes in porosity and water content along the longitudinal direction, away from the two heater ends, since there was also a thermal gradient from the heater ends towards the back and the front of the gallery (Figure 5).

Towards the shotcrete plug the water content tended to be higher than in the regions farther into the gallery, which could be because these sections had been subjected to heating during the 1st operational phase. Because of hysteresis effects, the water retention capacity of a material previously submitted to drying can be higher (Villar 2002). Also, some additional hydration with the water in the shotcrete could have taken place during the plug installation. Several factors could have contributed to the dry density decrease observed at the front of the barrier. On the one hand, this part of the barrier could have slightly moved towards the gallery entrance during the partial dismantling in 2002. But mostly the density decrease in this area could be related to the net 5-cm displacement of the bentonite slices towards the gallery entrance prompted by the shotcrete plug demolition in 2015 and the consequent stress release. In both cases the displacement of the bentonite slices was checked by measuring the x-coordinate and comparing it to the one measured for the same slices during installation.

## 5.3 Assessment of results

The bentonite dismantling operations took three months and started after the heater had been switched off for 14 days. During this time changes took place in the bentonite, and the state observed upon dismantling did not exactly reflect the state of the barrier during operation. The different processes that could have affected the barrier from shutdown to the water content and dry density determinations have to be identified, assessed and taken into account in the final evaluation. Thus, when analysing the water distribution in the barrier it has to be taken into account that when the sections were dismantled the temperature in them was lower than the temperatures during operation. This temperature change had surely an impact on the water distribution around the heater, where water in the vapour phase would condense because of cooling. Since the internal part of the barrier closest to the heater was not completely saturated, water movement from the external and middle, saturated part of the barrier towards the drier

inner part would be feasible and driven by the suction potential. This was already observed during the first dismantling, when relative humidity sensors were still working near the heater and the increase in relative humidity in this area upon switching-off was recorded (Villar et al. 2005, 2006). Because no relative humidity or suction sensors were working close to the heater during the final dismantling, it was not possible to evaluate the extent of this water redistribution, but it is very likely that the water content close to the heater was lower at the time of heater shutdown than was measured during dismantling. Nevertheless, the change in water content distribution upon heater shutdown would have been lower after eighteen years than after five years of operation, because the degree of saturation was much higher in the first case and the pore space available for water movement smaller.

Concerning the potential changes in the barrier dry density, the demolition of the shotcrete plug implied a release of stresses and an expansion of the bentonite towards the front of the gallery that could have yielded lower density values in the first sections sampled (sections S37 to S43) than the actual ones during operation. This effect attenuated towards the back of the gallery and probably did not affect the rest of the sections.

As well, sampling through core drilling and the trimming to prepare the subsamples for water content and density determination would introduce an additional decrease in dry density that would affect all the samples, but particularly those of higher water content. Hence, it is probable that the overall as-built dry density (and consequently degree of saturation) of the barrier was higher than the one measured.

## 6. Summary and conclusions

The FEBEX *in situ* experiment was a full-scale test reproducing the near-field of a nuclear waste repository performed at the Grimsel Test Site (GTS, Switzerland). The barrier was composed of FEBEX bentonite blocks. The thermal effect of the heat-generating canisters was simulated by means of two heaters whose surface temperatures were set to100°C, whereas hydration was natural by the granitic groundwater. The heating stage of the test began in 1997.

After five years of operation, half of the experiment was dismantled. The remaining part of the experiment continued running until 2015, when the final complete dismantling of the experiment was undertaken. Numerous samples of bentonite were taken in selected sections evenly distributed along the gallery for the on-site determination of dry density and water content. The main results obtained have been presented and discussed in this paper.

The on-site measurements showed that the physical state of the barrier after eighteen years of operation was very much affected by the processes to which it had been subjected, namely hydration from the granite and/or thermal gradient. The patterns observed are summarised below:

- All the gaps between blocks were sealed, both those among blocks of the same section and the gaps between adjacent bentonite sections. There was no effect of the vertical gaps between bentonite slices on the water content and dry density distribution, which proves that they were not preferential water pathways. The granite/bentonite contact was tight at all locations and the openings carved in the blocks for the passing of cables had been completely filled by the swelling of the bentonite. This was already observed during the partial dismantling after five years operation. The water availability at the test site (both in the liquid and the vapour phase) was enough to allow for quick swelling of the external part of the barrier. In turn, the quick swelling avoided preferential paths to remain open.

- The water content and dry density in every section followed a radial distribution around the axis of the gallery, with the water content decreasing from the granite towards the axis of the gallery and the dry density following the inverse pattern. The water content and density gradients were more noticeable in those sections affected by the heater.

- The measurements of the *x*-coordinate of the bentonite slices showed that the slices closest to the shotcrete plug moved towards the entrance of the gallery, which is assumed to have happened as the shotcrete plug was demolished and the swelling pressure (about 6 MPa at the shotcrete/bentonite interface) released. The net forward displacement of the slices decreased towards the back of the gallery. The sections of blocks at the back of the gallery

423 located beyond the heater moved in the opposite direction, probably during the operation
424 phase and in response to the less densely installed buffer and construction gaps at the back
425 of the gallery.

426 • There were also significant changes in dry density and water content along the axis of the
427 tunnel:

428 – The bentonite in the rear-most portion of the gallery contained the highest water
429 contents and the lowest dry densities. This was most probably caused by a larger
430 volume of construction gaps, which resulted in a lower installation density, a condition
431 that remained to some extend to the end of operation.

432 – The highest dry densities were found around the rear half of the heater and at its lower
433 part, where the temperatures were higher and the end-of-test water content lowest.

434 – Around the dummy canister dry densities below the average of the barrier were found.
435 This density decrease was related to the displacement of the slices towards the gallery
436 entrance upon plug demolition and pressure release. The bentonite around the dummy
437 canister had also been subjected to high thermal gradient during the 1$^{st}$ operational
438 phase but it was cool during the 2$^{nd}$ operational phase, which may have also affected its
439 condition.

440 When analysing the state of the barrier observed at the time of dismantling, the processes that
441 could have taken place between heater shutdown and the on-site measurements need to be
442 considered, in case the state of the barrier could have experienced changes with respect to the
443 actual one during operation. Thus, upon switching-off of the heater the barrier cooled down and
444 the thermal gradient disappeared. Hence, the water content of the bentonite in contact with the
445 heater was probably lower during operation than the values measured in the course of
446 dismantling, because of the possibility of water transfer triggered by cooling. Conversely, the
447 water content of the middle barrier ring in these areas could have been slightly higher during
448 operation than that measured. Additionally, the dry density and degree of saturation of the front

449 sections may have been higher during FEBEX operation than those measured, because of the
450 decompression and expansion of the bentonite experienced upon plug demolition. Finally,
451 sampling and trimming induced a decrease in the bentonite dry density and consequently, the
452 average dry density and degree of saturation of the barrier would be actually higher than the
453 measurements indicated. Nevertheless, the best estimates of the final average water content, dry
454 density and degree of saturation for the whole bentonite barrier were 25.5%, 1.59 g/cm$^3$ and
455 97%, respectively. The final average dry density along the barrier was lower than the initial
456 average value of 1.61 g/cm$^3$ (average value for the half of the experiment remaining in place
457 during the 2$^{nd}$ operational phase). This is attributed to the slight decompression suffered by the
458 barrier on dismantling and to the sampling procedures. The intrusion of bentonite into the void
459 between liner and heater could also have contributed to the decrease in the average dry density
460 of the barrier.

461 These results highlight the expansive potential of the bentonite, and its adequate performance
462 for a long period of time, even under thermal gradient. At the same time, the water content and
463 dry density gradients generated as a consequence of hydration and heating have proved to be
464 persistent, and maybe irreversible, since in this particular case, they were already observed after
465 five years of operation and have kept for other thirteen additional years, despite the fact that the
466 degree of saturation was overall quite high. Hence, a barrier of an initially homogeneous dry
467 density ended up having important inhomogeneities in terms of dry density and water content.
468 This could indicate that the volume changes induced during the initial saturation were
469 irreversible. Villar & Lloret (2007) stated that, according to laboratory tests with untreated
470 samples interpreted by generalised plasticity models (Lloret et al. 2003) and provided that the
471 net stresses in the barrier are not higher than the bentonite swelling pressure, these macroscopic
472 changes would be irreversible and the density heterogeneity through the barrier would remain.

473 These gradients have not impaired the performance of the barrier, but imply that the bentonite
474 barrier can be inhomogeneous and this will have a repercussion on its thermo-hydro-mechanical

properties, since most of them (thermal conductivity, swelling pressures, permeability, water retention, among others) depend greatly on the density and water content of the bentonite.

**Acknowledgements**

The FEBEX project was financed by ENRESA and the EC Contracts FI4W-CT95-006 and FIKWCT-2000-00016. The FEBEX-DP Consortium (NAGRA, SKB, POSIVA, CIEMAT, KAERI) financed the dismantling operation and on-site determinations in 2015. The support of the responsible person of the Consortium, Dr. Florian Kober, is greatly acknowledged. Cristina de la Rosa, Miguel Angel Manchón, Hector Abós and Victor Martínez from AITEMIN performed the on-site laboratory work. The BEACON project, which receives funding from the Euratom research and training programme 2014-2018 under grant agreement No 745942, financed the preparation of this paper.

**References**

AITEMIN, CIEMAT, CSIC-Zaidín, TECNOS, ULC, UPC-DIT, UPM. 1998. FEBEX. Pre-operational stage summary report. Publicación Técnica ENRESA 01/98. ENRESA, Madrid. 185 pp.

AITEMIN. 2003. Sensors Data Report (In Situ Experiment). Project Deliverable D8-d. Report n.30. Technical Report 70-AIT-L-6-07. Madrid, 178 pp.

Bárcena, I, García-Siñeriz, J.L. 2015. FEBEX-DP (GTS) Full Dismantling Sampling Plan (in situ Experiment). Nagra Arbeitsbericht NAB 15-14. 103 pp.

Bárcena, I., Fuentes-Cantillana, J.L., García-Siñeriz, J.L. 2003. Dismantling of the heater 1 at the FEBEX *in situ* test. Description of Operations. Publicación Técnica ENRESA 09/2003, Madrid, 134 pp.

Chapman, N., McCombie, C. 2003. Principles and Standards for the Disposal of Long-Lived Radioactive Wastes. *Waste Management Series* 3, Elsevier, Amsterdam. 270 pp.

Daucausse, D. & Lloret, A. 2003. Results of “in situ” measurements of water content and dry density. FEBEX report 70-UPC-L-5-012. 85 pp. Barcelona.

ENRESA 2006. FEBEX Full-scale Engineered Barriers Experiment, Updated Final Report 1994-2004. Publicación Técnica ENRESA 05-0/2006, Madrid, 590 pp.

Fuentes-Cantillana, J.L., García-Siñeriz, J.L. 1998. FEBEX. Final design and installation of the “in situ” test at Grimsel. Publicación Técnica ENRESA 12/98. Madrid, 184 pp.

García-Siñeriz, J.L, Abós, H., Martínez, V., de la Rosa, C., Mäder, U., Kober, F. 2016. FEBEX-DP: Dismantling of the heater 2 at the FEBEX "in situ" test. Description of operations Nagra Arbeitsbereicht NAB16-011. Wettingen, 92 pp.

Kober, F., van Meir, N. 2017. FEBEX-DP – Dismantling related supplementary documents. Nagra Arbeitsbericht NAB 16-068. Wettingen, 15 pp, 8 Annexes.

Lanyon, G.W. & Gaus, I. 2016. Main outcomes and review of the FEBEX In Situ Test (GTS) and Mock-Up after 15 years of operation. Nagra Arbeitsbericht NAB 15-04, 79 pp.

Lloret, A., Villar, M.V., Sánchez, M., Gens, A., Pintado, X., Alonso, E.E. 2003. Mechanical behaviour of heavily compacted bentonite under high suction changes. Géotechnique 53(1): 27-40.

Martínez, V., Abós, H., García-Siñeriz, J.L. 2016. FEBEXe: Final Sensor Data Report (FEBEX “in situ” Experiment). Nagra Arbeitsbereicht NAB 16-019. Wettingen, 244 pp.

Vardon, P.J., Heimovaara, T.J. 2017. Waste barriers in environmental geotechnics. Environmental Geotechnics 4(6): 390-392.

Villar, M.V. 2002. Thermo-hydro-mechanical characterisation of a bentonite from Cabo de Gata. A study applied to the use of bentonite as sealing material in high level radioactive waste repositories. Publicación Técnica ENRESA 01/2002. 258 pp. Madrid.

522 Villar, M.V.& Lloret, A. 2007. Dismantling of the first section of the FEBEX *in situ* test: THM
523 laboratory tests on the bentonite blocks retrieved. Physics and Chemistry of the Earth,
524 Parts A/B/C 32 (8-14): 716-729.

525 Villar, M.V., García-Siñeriz, J.L., Bárcena I., Lloret, A. 2005. State of the bentonite barrier after
526 five years operation of an *in situ* test simulating a high level radioactive waste
527 repository. Engineering Geology 80(3-4): 175-198.

528 Villar, M.V. (ed.) 2006. FEBEX Project Final report. Post-mortem bentonite analysis.
529 Publicación Técnica ENRESA 05-1/2006. ENRESA, Madrid. 183 pp. ISSN 1134-
530 380X.

531 Villar, M.V.; Iglesias, R.J.; Abós, H.; Martínez, V.; de la Rosa, C. & Manchón, M.A. 2016.
532 FEBEX-DP onsite analyses report. Nagra Arbeitsbereicht NAB 16-012. Wettingen, 101
533 pp.

534

535 **Table 1: Average properties for each section as computed from the contour plots and the**
536 **fitting of polynomial functions (see Figure 3 for location of sections)**

| *x*-coordenate (mm) | Sampling section | Contour plots | | | Polynomial functions | | |
|---|---|---|---|---|---|---|---|
| | | *w* (%) | $\rho_d$ (g/cm$^3$) | $S_r$ (%) | *w* (%) | $\rho_d$ (g/cm$^3$) | $S_r$ (%) |
| 8455 | S37 | 28.3 | 1.55 | 103 | 27.9 | 1.56 | 103 |
| 9214 | S39 | 27.7 | 1.54 | 100 | 27.3 | 1.56 | 100 |
| 10107 | S43 | 27.3 | 1.59 | 106 | 27.0 | 1.59 | 105 |
| 11112 | S45 | 25.0 | 1.59 | 97 | 24.9 | 1.60 | 97 |
| 12265 | S49 | 25.0 | 1.60 | 98 | 25.0 | 1.60 | 98 |

| *x*-coordenate (mm) | Sampling section | Contour plots | | | Polynomial functions | | |
|---|---|---|---|---|---|---|---|
| | | *w* (%) | $\rho_d$ (g/cm$^3$) | $S_r$ (%) | *w* (%) | $\rho_d$ (g/cm$^3$) | $S_r$ (%) |
| 13413 | S52 | 24.8 | 1.59 | 95 | 25.0 | 1.59 | 97 |
| 14555 | S56 | 26.1 | 1.57 | 98 | 26.2 | 1.57 | 98 |
| 15695 | S58 | 27.2 | 1.55 | 98 | 26.9 | 1.55 | 98 |
| 16870 | S61 | 32.7 | 1.46 | 103 | 32.4 | 1.46 | 103 |

537

538

539 **Figure captions**

540 Figure 1: Initial configuration of the FEBEX *in situ* test (dimensions in m). The arrow
541 indicates the area dismantled in 2002 (modified from AITEMIN *et al*. 1998)

542 Figure 2: Initial (1997) and final (2015) appearance of the bentonite barrier around the
543 heater (the circles on the right picture indicate the sampling positions)

544 Figure 3: General layout of the *in situ* test during the 2$^{nd}$ operational phase and location
545 along the gallery of the sampling sections used for bentonite water content and dry
546 density on-site determinations

547 Figure 4: Steady temperatures measured during operation by thermocouples located in
548 different instrumented sections (see Figure 3 for location of sections)

549 Figure 5: Steady temperatures along the gallery axis measured during operation by
550 thermocouples located in different instrumented sections. The distance of the sensors to

551 the gallery axis is indicated in the legend. The position of the sampling sections along
552 the gallery is indicated by thick dotted vertical lines

553 Figure 6: Evolution of temperatures (ºC) in Section S54 (references and distances to
554 gallery axis of each sensor indicated in the legend) during a time period from before the
555 heater switching-off to just before dismantling of the section (modified from Martínez
556 et al. 2016)

557 Figure 7: Appearance of the void left after extraction of Heater #2 showing the
558 bentonite intruded through the liner holes (left) and bentonite adhered to granite
559 showing striation parallel to the axis of the gallery (indicated by an arrow, right)

560 Figure 8: Water content and dry density measured in subsamples taken along the six
561 sampling radii in section S49

562 Figure 9: Water content and dry density measured in subsamples taken along the six
563 sampling radii in section 58

564 Figure 10: Contour map for water content in section S45 (left) and S56 (right)

565 Figure 11: Contour map for dry density in section S45 (left) and S56 (right)

566 Figure 12: Comparison of the water content and dry density in a section around the
567 heater and away from it

568 Figure 13: Contour plot of water content in the vertical longitudinal section

569 Figure 14: Contour plot of dry density in the vertical longitudinal section

570 Figure 15: Average water content (w.c.) and dry density (d.d.) for the sections sampled
571 along the barrier as computed from the polynomial functions (Table 1)

572

573

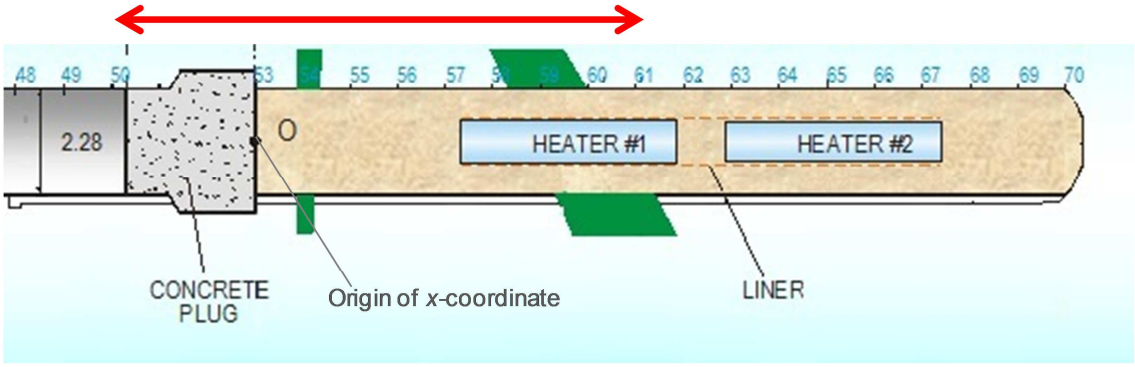


**Figure 1: Initial configuration of the FEBEX *in situ* test (dimensions in m). The arrow indicates the area dismantled in 2002 (modified from AITEMIN *et al*. 1998)**

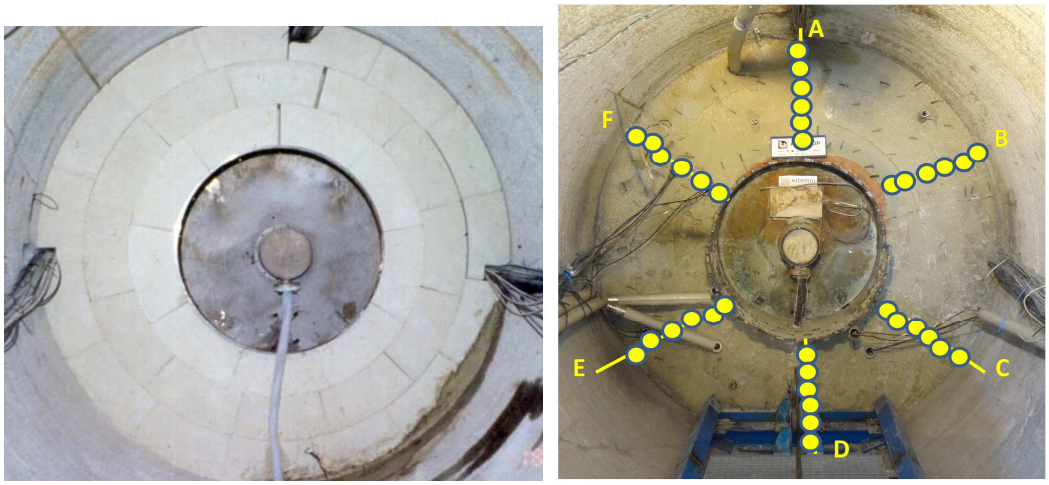


**Figure 2: Initial (1997) and final (2015) appearance of the bentonite barrier around the heater (the circles on the right picture indicate the sampling positions)**

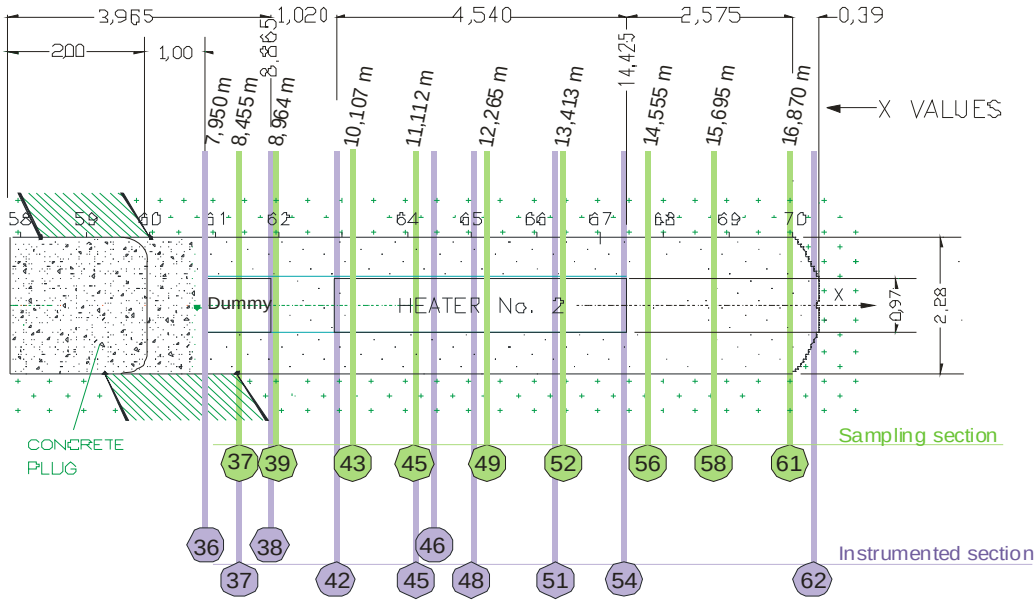


**Figure 3: General layout of the *in situ* test during the 2nd operational phase and location along the gallery of the sampling sections used for bentonite water content and dry density on-site determinations**

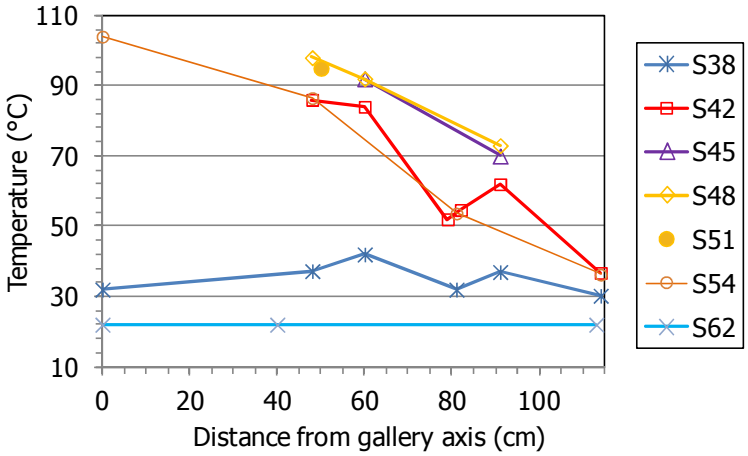


**Figure 4: Steady temperatures measured during operation by thermocouples located in different instrumented sections (see Figure 3 for location of sections)**

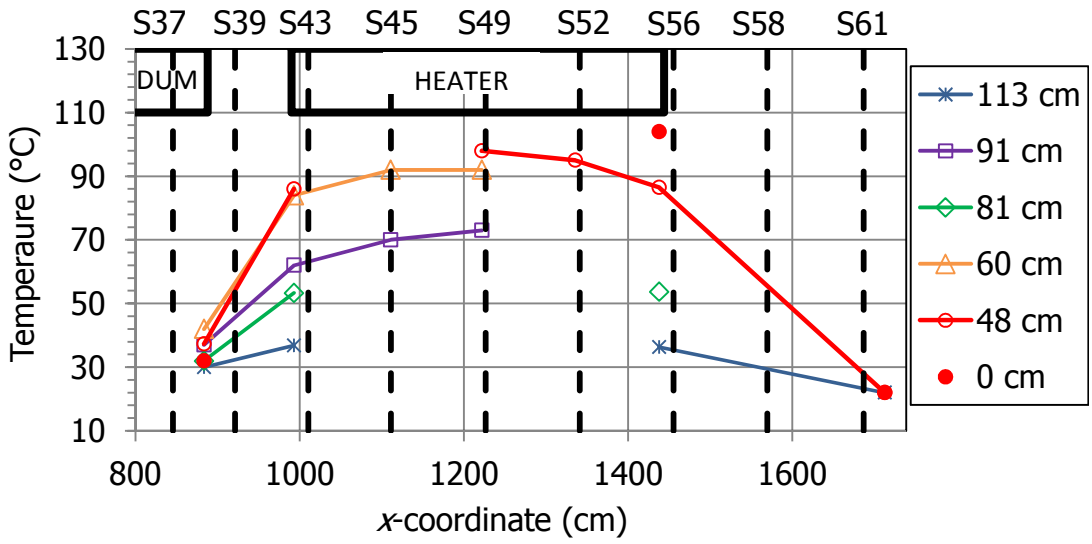


**Figure 5: Steady temperatures along the gallery axis measured during operation by thermocouples located in different instrumented sections. The distance of the sensors to the gallery axis is indicated in the legend. The position of the sampling sections along the gallery is indicated by thick dotted vertical lines**

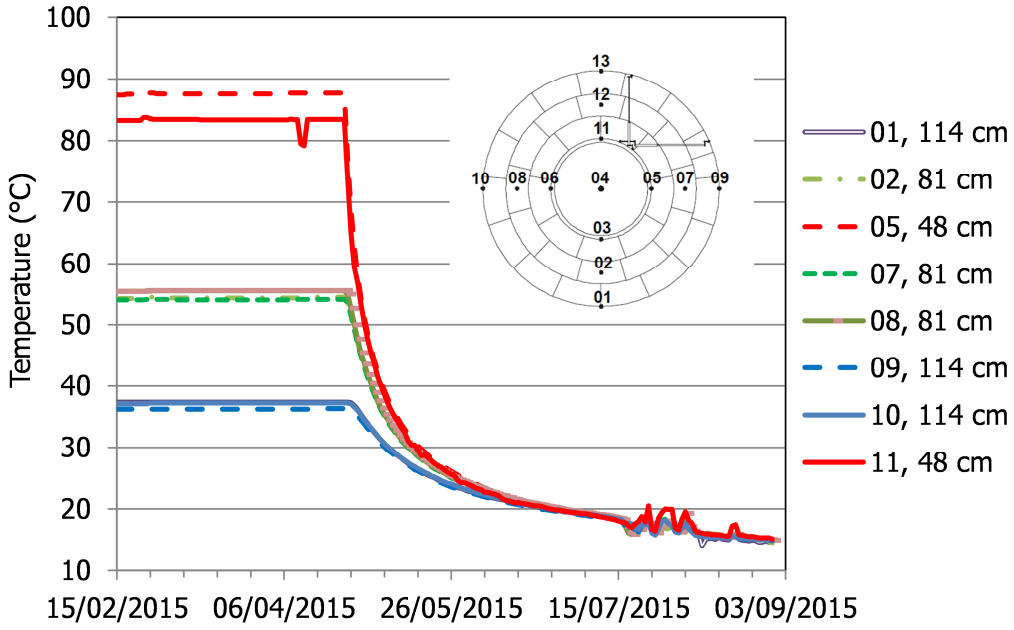


**Figure 6: Evolution of temperatures (ºC) in Section S54 (references and distances to gallery axis of each sensor indicated in the legend) during a time period from before the heater switching-off to just before dismantling of the section (modified from Martínez et al. 2016)**

**Figure 7: Appearance of the void left after extraction of Heater #2 showing the bentonite intruded through the liner holes (left) and bentonite adhered to granite showing striation parallel to the axis of the gallery (indicated by an arrow, right)**

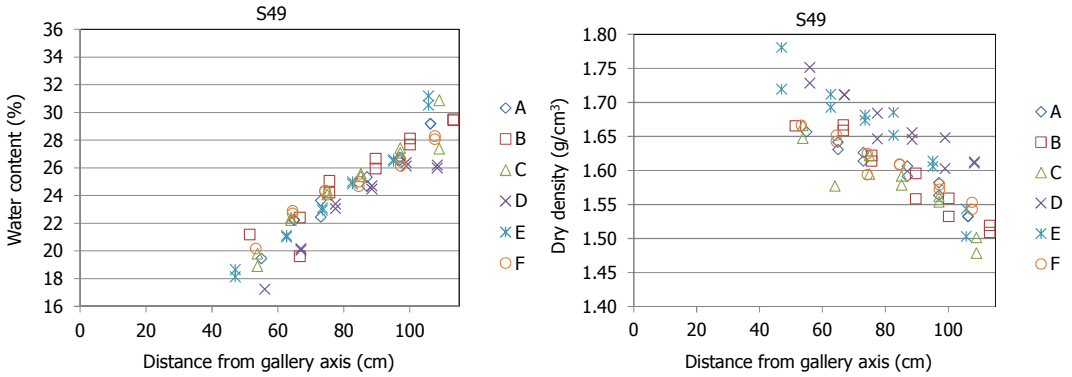


**Figure 8 Water content and dry density measured in subsamples taken along the six sampling radii in section S49**

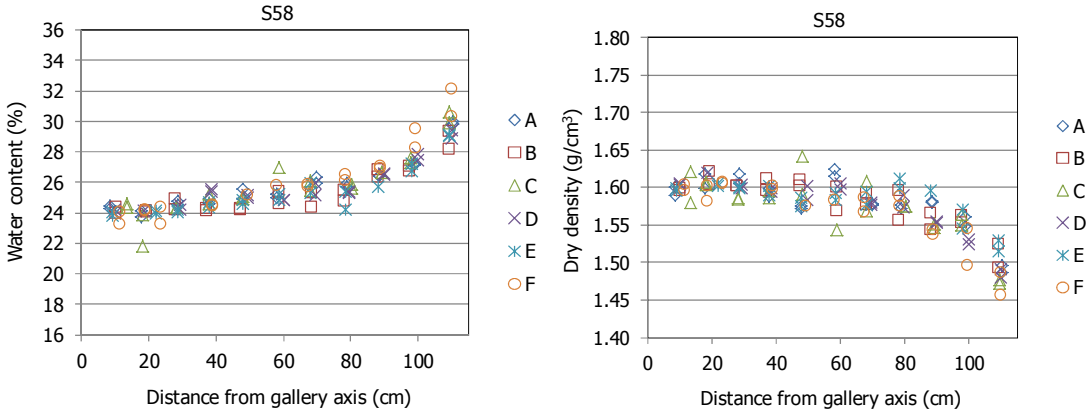


**Figure 9 Water content and dry density measured in subsamples taken along the six sampling radii in section 58**

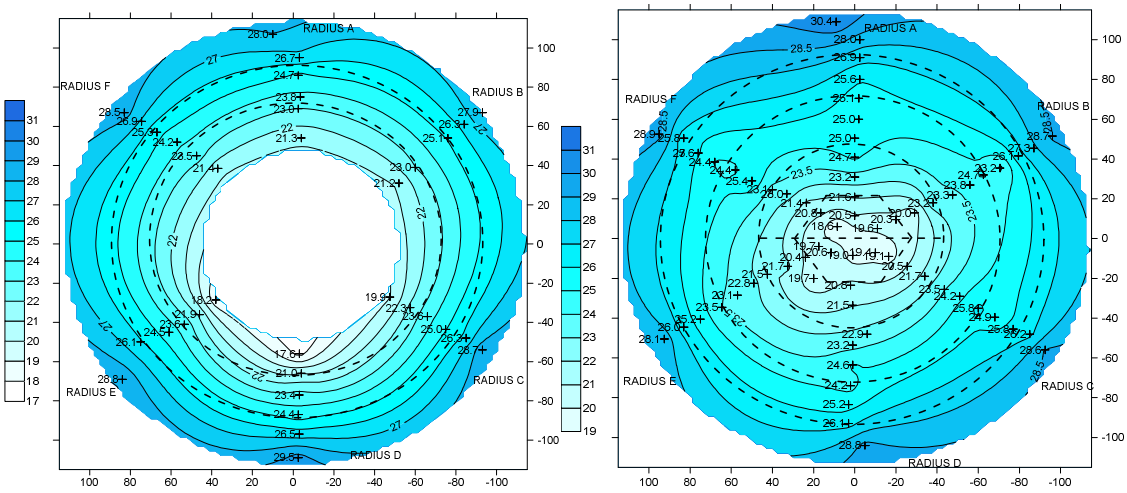


**Figure 10: Contour map for water content in section S45 (left) and S56 (right)**

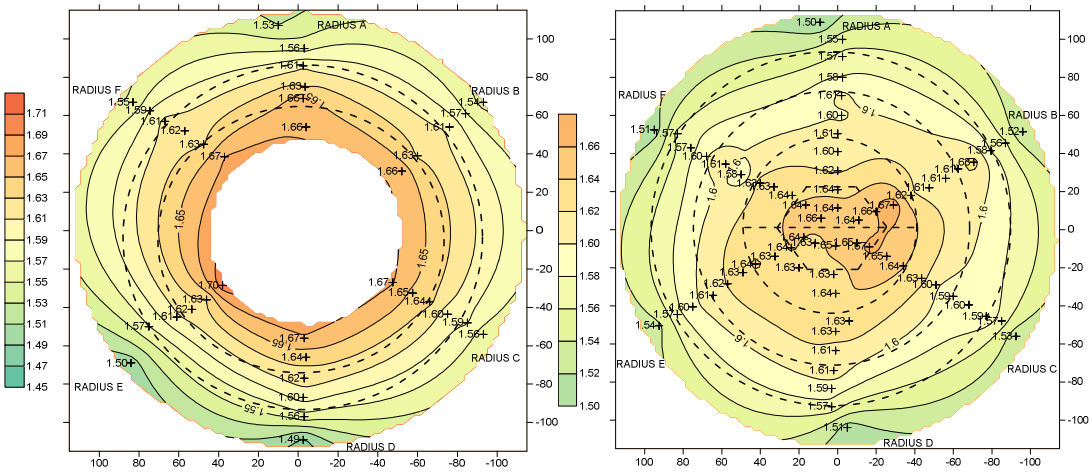


**Figure 11: Contour map for dry density in section S45 (left) and S56 (right)**

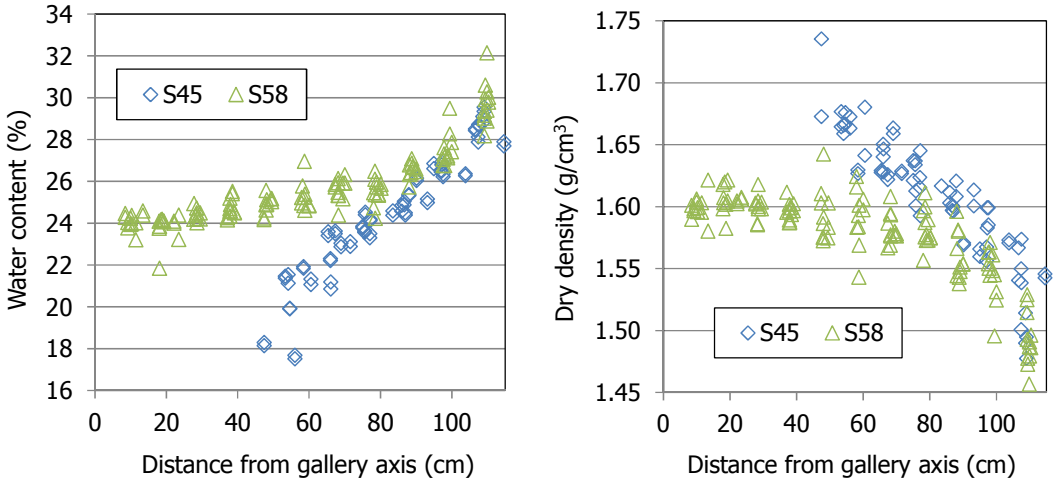


**Figure 12: Comparison of the water content and dry density in a section around the heater and away from it**

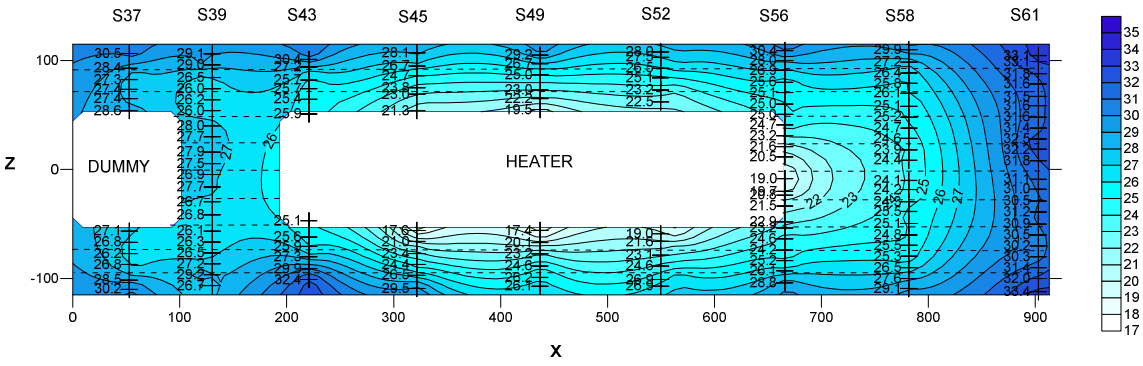


**Figure 13: Contour plot of water content in the vertical longitudinal section**

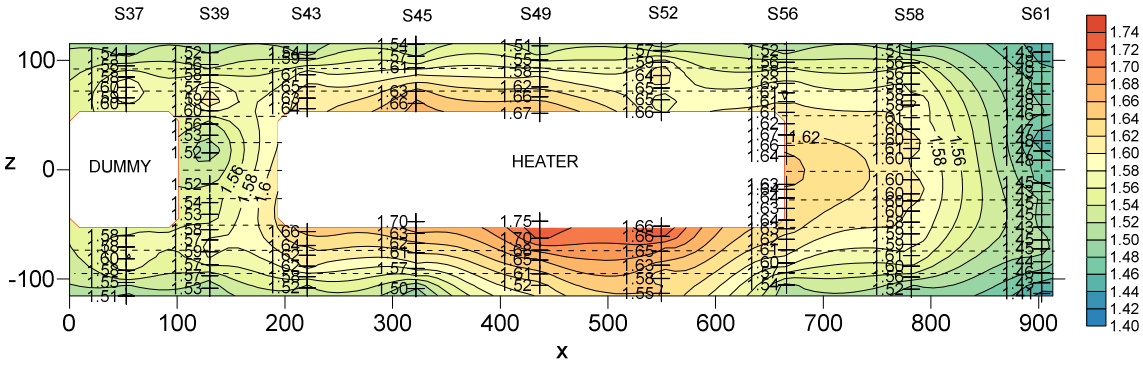


**Figure 14: Contour plot of dry density in the vertical longitudinal section**

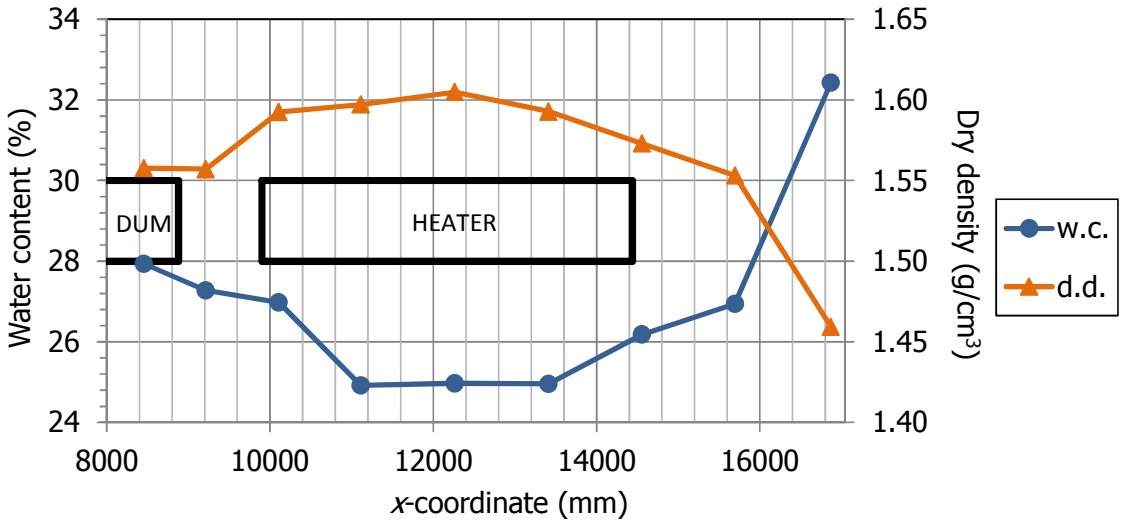


**Figure 15 Average water content (w.c.) and dry density (d.d.) for the sections sampled along the barrier as computed from the polynomial functions (Table 1)**